Online database of clinical MR and ultrasound images of brain tumors

Laurence Mercier
McConnell Brain Imaging Centre, Montreal Neurological Institute, McGill University, Montreal H3A 2B4, Canada

Rolando F. Del Maestro and Kevin Petrecca
Brain Tumour Research Centre, McGill University, Montreal H3A 2B4, Canada and Department of Neurology and Neurosurgery, Montreal Neurological Institute, McGill University, Montreal H3A 2B4, Canada

David Araujo
McConnell Brain Imaging Centre, Montreal Neurological Institute, McGill University, Montreal H3A 2B4, Canada

Claire Haegelen
McConnell Brain Imaging Centre, Montreal Neurological Institute, McGill University, Montreal H3A 2B4, Canada; INSERM, U746, Faculty of Medicine, University of Rennes I, Rennes, France; INRIA, VisAGeS Unit/Project, University of Rennes I, Rennes, France; and CNRS, UMR 6074, IRISA, University of Rennes I, Rennes, France

D. Louis Collins[a)]
McConnell Brain Imaging Centre, Montreal Neurological Institute, McGill University, Montreal H3A 2B4, Canada

(Received 16 November 2011; revised 8 April 2012; accepted for publication 10 April 2012; published 22 May 2012)

Purpose: One of the important challenges in the field of medical imaging is finding real clinical images with which to validate new image processing algorithms. This is particularly true for tracked 3D ultrasound images of the brain.
Methods: In 2010, pre- and postoperative magnetic resonance and intraoperative ultrasound images were acquired from brain tumor patients involved in the authors' imaging study at the Montreal Neurological Institute.
Results: These data are available online at the Montreal Neurological Institute's Brain Images of Tumors for Evaluation database, termed here the MNI BITE database. It contains ultrasound and magnetic resonance images from 14 patients. Each patient underwent a preoperative and a postoperative T1-weighted magnetic resonance scan with gadolinium enhancement, and multiple intraoperative B-mode images were acquired before and after resection. Corresponding features were manually selected in some image pairs for validation. All images are in MINC format, the file format used at the authors' institute for image processing. The MINC tools are available for free download at packages.bic.mni.mcgill.ca.
Conclusions: This is the first online database of its kind. These images can be used by image processing scientists as well as clinicians wishing to compare findings from magnetic resonance and ultrasound imaging.
[http://dx.doi.org/10.1118/1.4709600]

Key words: online database, intraoperative ultrasound, MRI, brain tumors, validation, registration

I. INTRODUCTION

One of the biggest challenges faced by computer scientists and engineers in the field of medical imaging is finding real clinical images with which to validate new image processing algorithms. For example, technical laboratories are rarely located within hospitals, which can make it difficult to obtain access to clinical data. Moreover, it is often impossible to find neurosurgeons and/or neuroradiologists who are willing to take the time to provide their expertise in terms of gold standard data for the validation of technical algorithms.

In 2010, patients undergoing brain tumor surgery with two neurosurgeons (R.D.M. and K.P.) at the Montreal Neurological Institute (MNI) and Hospital consented to the online publication of their anonymized MR and ultrasound images for the benefit of the scientific community (MNI's ethics approval: NEU-09-010). Each of the 14 patients enrolled in our study underwent pre- and postoperative T1-weighted (T1w) magnetic resonance (MR) scans with gadolinium enhancement. Each patient also had multiple intraoperative B-mode ultrasound images acquired pre- and postresection. The intraoperative ultrasound images were tracked, which facilitates the comparison of various brain structures and lesion(s) with the MR images. Homologous landmarks were manually selected in some image pairs for validation. These data are available online at the Montreal Neurological Institute's Brain Images of Tumors for Evaluation database, termed here the MNI BITE database.[40]

Our database was inspired by other online databases for medical imaging studies, some of which focus on simulated or phantom images. Two examples of numerically simulated databases include TumorSim, which provides simulated MR images of brain tumors[1] for the validation of segmentation methods, and BrainWeb, which contains simulated MR images of the brain for both normal anatomy and data from patients with multiple sclerosis (MS).[2,3] Chen *et al.*[4] created a database of computed tomography, MR, and ultrasound images of a physically realistic tissue mimicking brain phantom, designed for the validation of new image processing methods such as segmentation, reconstruction, registration, and denoising.

Other available databases provide real *in vivo* images of normal controls or patients with certain pathologies, and some of these databases include manual segmentation of certain neuroanatomical structures. Examples include the Internet Brain Segmentation Repository (IBSR),[5] which contains manually segmented MR images of the brain for the validation of new segmentation methods, and the LONI Probabilistic Brain Atlas (LPBA40), created from 40 MR images of normal brains on which 56 structures were manually identified.[6] The BrainMap database[7] contains published functional neuroimaging [functional MR imaging and positron emission tomography (PET)] experiments in Talairach space. The National Institutes of Health-funded study of normal brain development (NIHPD) provides over 500 MR images of normal children for the study of normal brain development.[8] The whole brain atlas[9] features images of normal brains and those with various pathologies as an introduction to neuroanatomy. The Alzheimer's Disease Neuroimaging Initiative (ADNI) database[10] provides MR and PET images of the brain with the goal of promoting a better understanding of the progression of Alzheimer's disease. The Open Access Series of Imaging Studies (OASIS) contains a large number of MR images of the brains of normal and demented adults.[11,12]

The availability of medical image databases online enables the development, evaluation, and comparison of different algorithms. Because they provide a common set of data, online databases also allow direct comparison of different image processing methods. The value of these databases cannot be underestimated: Without common data, direct comparison of image processing methods is impossible. For example, the BrainWeb database has been cited over 600 times and has been used to validate tissue classification algorithms, cortical surface extraction, deep brain structure segmentation, and MS lesion algorithms. The BrainMap database now counts over 2100 associated publications.

The online database presented here is the first of its kind: the first to include intraoperative ultrasound of the brain and the first to include pre- and postresection MR images of neurosurgical patients. These images can be used by both image processing scientists and clinicians wishing to compare MR and ultrasound findings. Our goal is that our database will trigger multiple studies, which we hope will eventually lead to more complete brain tumor resections to, ultimately, prolong patient survival.

II. MATERIALS AND METHODS

II.A. Clinical data

Table I summarizes the brain tumor cases included in this project. Five women and nine men consented to participate, with a mean age of 52 years. As the most common type of primary brain tumor, gliomas were the only type of tumor included in our study. For nonclinical readers, the malignancy of a glioma is expressed using a grading system from I to IV. A grade I glioma is a benign tumor, more common in children than adults (none included here). Low-grade

TABLE I. Overview of brain tumor cases included in this study. From left to right, columns indicate: patient number, sex and age of each patient, hemisphere and lobe in which the tumor was located, general tumor type: either low-grade glioma (LGG) or high-grade glioma (HGG), specific tumor type: astrocytoma (astro), oligodendroglioma (oligo), or glioblastoma (GBM) and grade (gr), estimated tumor volume, patient's first, or reoperation (redo).

Patient No.	Sex	Age	Tumor location	Tumor type	Grade	Tumor vol (cm^3)	First or redo
1	F	42	Right frontal	HGG	GBM	2.3	First
2	M	31	Right frontal	LGG	Astro gr. II[a]	79.2	First
3	M	70	Left parietotemporal	HGG	GBM	53.7	First
4	M	72	Right parietal	HGG	GBM	31.6	First
5	M	39	Left frontal	HGG	Oligo gr. III + cyst	0.2[b]	Redo
6	M	40	Left frontal	HGG	GBM	32.3	Redo
7	M	62	Left temporal	HGG	GBM	13.9	Redo
8	M	23	Left frontal	LGG	Oligo gr. II	66.0	Redo
9	F	42	Left frontal	HGG	GBM	4.8	First
10	F	49	Left frontal	HGG	Oligo gr. III	10.4	Redo
11	F	40	Right frontal	LGG	Astro gr. II	39.7	First
12	F	72	Left frontal	HGG	GBM[c]	49.1	First
13	M	76	Right parietal	HGG	GBM	31.9	Redo
14	M	70	Right temporal	LGG	Astro gr. II	37.7	First
Mean		52				30	

[a]This patient had a second tumor in the other hemisphere. The right frontal tumor was the goal of the surgery.
[b]The tumor volume for this case did not include the cyst.
[c]Multifocal GBM. The left frontal part was the goal of the surgery.

gliomas are malignant tumors of grade II; high-grade gliomas are ranked grade III or IV. Our study included four low-grade and ten high-grade gliomas. Table I further divides gliomas into subtypes: astrocytomas (astro), oligodendrogliomas (oligo), and glioblastomas (GBM). Glioblastomas are the most common and aggressive type of gliomas (grade IV). The tumors included in this study were all supratentorial, with the majority in the frontal lobe (9/14). The mean tumor volume computed from a manual slice-by-slice segmentation on the preoperative MR images was 30 cm^3. Eight patients were undergoing their first operation, and six, a reoperation, which means that some had resection corridors and/or resection cavities from previous surgeries.

II.B. MR images

The preoperative MR images were global T1w gadolinium-enhanced MR images. Except for that of patient #8, all preoperative images were acquired on a 1.5 T GE Signa EXCITE (General Electric, Milwaukee, WI) with 1 mm slice thickness and 0.5×0.5 mm^2 in-plane pixel size [three-dimensional (3D) axial SPGR sequence, TE = 8 ms, TR = 23 ms, flip angle = 20°]. Patient #8 had his preoperative MR scan on a 3 T Tim-Trio (Siemens Medical Solutions, Erlangen, Germany) with 1 mm slice thickness and 1×1 mm^2 in-plane pixel size (sagittal 3D MPRAGE acquisition, TE = 3.43 ms, TR = 2.3 s, flip angle = 9°). The preoperative MR images were acquired on average 17 days before surgery (range = 1–72 days). Table II gives some information about the MR images available for each case. The postoperative MR images were also T1w gadolinium-enhanced MR images with 0.5×0.5 mm^2 in-plane pixel size (3D axial SE sequence, TE = 8 ms, TR = 23 ms, flip angle = 20°), but varying slice thicknesses (see last column of Table II). The images were acquired less than 48 h after surgery (mean = 1.3 days). Patient #13 underwent a postoperative computed tomography scan and no postoperative MR scan.

TABLE II. Information about the MR images included in this study. First column is the patient number. Second column is the number of days between the preoperative MR scan (MRI) and the surgery. Third column is the number of days between the surgery and the postoperative MR scan. Fourth column is the slice thickness of the postoperative MR image.

Patient No.	Days, MRI–OR	Days, OR–MRI	Slice thickness postoperative MRI (mm)
1	6	1	2.0
2	1	2	2.0
3	18	2	2.0
4	10	1	2.0
5	72	1	5.5
6	9	2	2.0
7	1	1	2.0
8	36	1	2.0
9	17	1	5.5
10	5	2	2.0
11	5	2	1.0
12	6	0	1.0
13	3	–	–
14	47	1	1.0
Mean	17	1.3	

All MR images were converted to the MINC format,[13] the format used at our institute for image processing. MINC tools can be found at packages.bic.mni.mcgill.ca. The only preprocessing applied to the MR images was anonymization of their headers. The images were not corrected for intensity nonuniformities nor normalized in any way. Many preprocessing methods exist, and we did not want to assume what would be best for all users.

II.C. Ultrasound image acquisition and processing

We used our prototype neuronavigation system, IBIS NeuroNav, to acquire the intraoperative ultrasound images. The precision and accuracy of many of IBIS's components were estimated in Mercier *et al.*[14] The IBIS NeuroNav system consists of a computer connected to an ultrasound machine and a tracking device. The computer used to acquire the ultrasound images was a dual-core Intel Xeon 3 GHz processor running Debian GNU-Linux 3.1. The ultrasound machine was an HDI 5000 (ATL/Philips, Bothell, WA), and the ultrasound probe was a P7-4 MHz phased array transducer. The ultrasound probe was tracked with reflective spheres rigidly fixed to a TA003 tracker (Traxtal Technologies Inc., Toronto, Ontario, Canada) by a Polaris infrared optical system (Northern Digital, Waterloo, Ontario, Canada) (see Fig. 1). To calibrate the ultrasound probe, a calibration phantom with four Z-fiducials was used,[15] enabling the accurate estimation of the x,y,z location in the camera space of each i,j pixel in the ultrasound images. As the probe cannot be sterilized, it was draped in a plastic sleeve, and the sterile spheres were clipped over the sleeve (see Fig. 1). Sterile gel was applied inside the sleeve at the end of the probe to facilitate acoustic coupling.

Ultrasound depth settings were 6.5 or 8 cm. The gain was adjusted independently for each case in order to obtain the best tumor contrast, which was generally achieved by raising the gain until the surrounding brain appeared in gray tones instead of blackish.

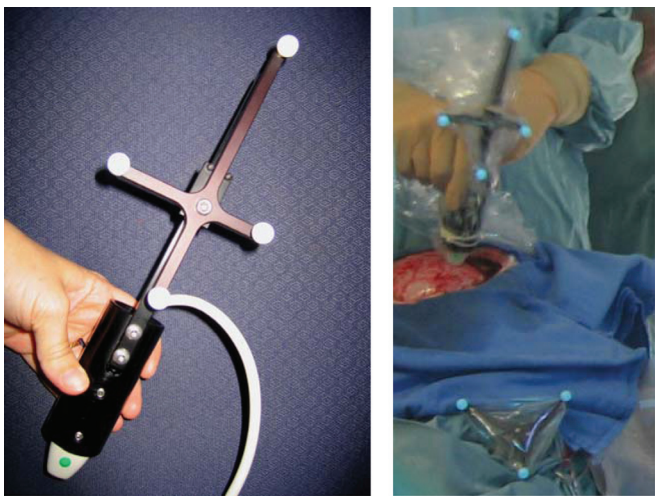

FIG. 1. Left: ultrasound probe with tracker. Right: probe draped for surgery and image acquisition on the dura.

The surgeon acquired the freehand ultrasound images in sweeps of typically 200 to 600 two-dimensional (2D) images, where a sweep is a series of 2D images acquired by slowly (rate of ~2–3 mm/s) moving the probe along one plane (i.e., no zigzag) with a continuous forward motion. This technique was used to minimize artifacts due to calibration errors. When a sweep was acquired too quickly, it contained bands of missing data. The surgeons (R.D.M. and K.P.) were trained by the engineer (L.M.) to achieve the optimal probe velocity and trajectory for 3D reconstruction. Whenever possible, for example, if the opening was large enough, the surgeon acquired additional sweeps using a slightly different path or angle, with the goal of covering as much anatomy as possible. In the database, the sweeps were not combined; each sweep was stored in a separate volume. The ultrasound images were transferred to the computer through a Pinnacle PCTV frame-grabbing card (Pinnacle Systems, Inc., Mountain View, CA). The sweeps of 2D images were then reconstructed in a 3D volume using a pixel-based method[16] that maps each pixel from each 2D image onto a regular 3D grid using trilinear interpolation. If no pixel covers a given voxel, it is set to zero. The resulting gaps must be masked out during the registration process.

Ultrasound images were acquired at two different time points, before and after the surgical resection of the tumor, with at least two sweeps at each time point. Ideally, preresection ultrasound images were acquired on the dura in a mostly translational motion, with a slight rotation at each extremity if the tumor was not entirely covered by the strict translational motion. Again, the translational motion of the probe minimizes probe calibration error. Imaging on the dura was possible when the patient was being operated on for the first time or the dura was used to close the cavity from a previous surgery. Otherwise, the surgeon imaged either directly on the cortex (or tumor) or on a dural repair patch (Dura-Guard, Synovis Surgical Innovations, MN) applied on the cortex. The surgeon irrigated the surface with saline to maintain acoustic coupling. For the postresection images, the cavity was filled with saline for coupling after first being rinsed to remove as much blood as possible. Images were acquired directly inside the resection cavity whenever possible. However, in some cases, the surgical cavity was in the shape of a "C" rather than a "U," making it impossible to fill with saline. The other option was to close the cavity with Dura-Guard, which then retained the saline inside the cavity for imaging. As a result, some patients have images acquired inside the cavity only; other patients have images acquired on the dura only, and some have images acquired in both locations.

For each ultrasound sweep, the database includes both the original tracked 2D ultrasound images and the reconstructed 3D ultrasound volume. This gives the possibility to reconstruct new 3D volumes using different parameters. The pixel size of the 2D ultrasound is 0.2×0.2 mm^2, and the voxel size in the 3D reconstructed ultrasound is $0.3 \times 0.3 \times 0.3$ mm^3. The ultrasound images are in MINC format. The MINC format contains the tracking information in its header.

II.D. Brain tumor characteristics on MR and ultrasound images

Technical medical imaging scientists might not be familiar with the appearance of brain tumors on MR and ultrasound images. We believe that a basic understanding of tumor imaging characteristics may help in the development of image processing algorithms, and we aim to provide that here.

Figure 2 shows examples of MR images of different glioma types. Grade II gliomas (Fig. 2, left) do not usually show any gadolinium enhancement. Their intensity often resembles that of gray matter, which is darker than the surrounding white matter. Their contour cannot always be clearly delimited.[17] The grade III glioma (Fig. 2, center) has a large resection cavity from a previous operation. Grade III gliomas can be fully enhancing (i.e., bright due to gadolinium enhancement) or show only some areas of enhancement. Grade IV gliomas (Fig. 2, right) commonly have both areas of enhancement and areas of necrosis (dead cells). Necrosis indicates fast growing tumors. The grade IV tumor shown in the rightmost panel of Fig. 2 also has surrounding edema.

Figure 3 shows examples of ultrasound images of different glioma types. In ultrasound images, tumors generally appear hyperechoic (brighter than the surrounding brain).[17–19] However, the intensity of the signal does not appear to be

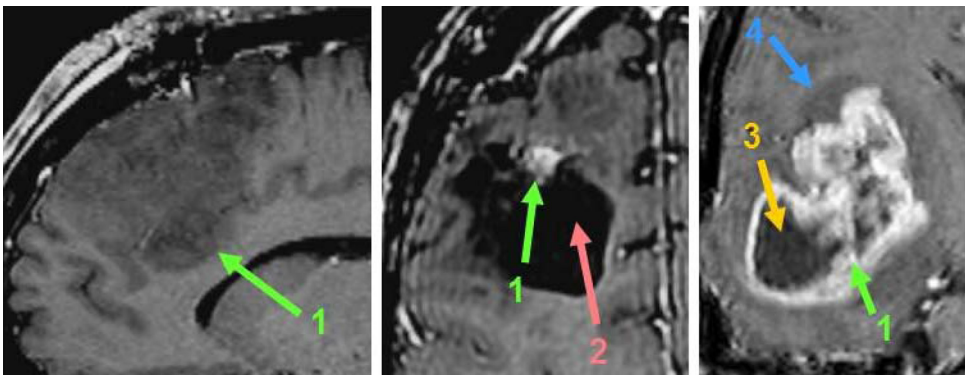

FIG. 2. T1w MR images of gliomas. Left: grade II glioma (patient #2). Center: grade III glioma with cyst (patient #5). Right: grade IV glioma (patient #3). The colored numbers correspond to the following: (1) tumor, (2) resection cavity from previous operation, (3) necrosis, and (4) edema.

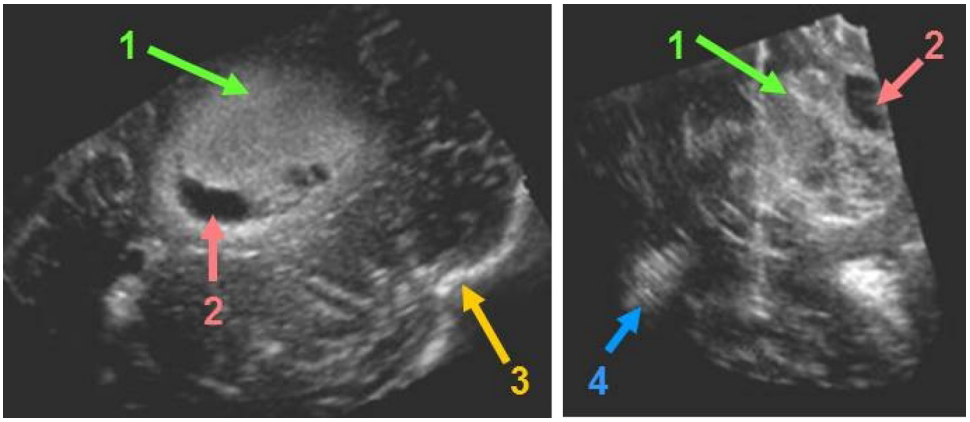

FIG. 3. Ultrasound images of gliomas. Left: grade II glioma (patient #11). Right: grade IV glioma (patient #4). The colored numbers correspond to the following: (1) tumor, (2) cystic component, (3) bone, and (4) choroid plexus.

correlated with tumor malignancy,[20] which is what we found in our study: the high- and low-grade tumors could not be differentiated based on their echogenicity. In ultrasound images, cerebrospinal fluid, cysts, and the liquid components of necrosis appear hypoechoic (darker than the surrounding brain). Blood appears more hyperechoic than other liquids because of the presence of ultrasound scatterers. In the literature, edema is described as either having an intensity in between that of the tumor and normal brain or not discernible from normal brain.[17]

Registration experts might benefit from the knowledge that the tumor characteristics in ultrasound and MR images are not always an exact match. For example, necrosis always has a dark signal intensity on T1-weighted MR images. On ultrasound, it will depend on whether the necrosis is more liquid (hypoechoic) or solid (hyperechoic). Similarly, tumor volumes/contours do not always match perfectly,[18] possibly because MR and ultrasound images are based on different physical properties, and, consequently, the borders of edema and infiltrative tumors like gliomas could be slightly different in the two modalities. In addition, as seen in Table II, MR and ultrasound images were acquired on average 17 days apart, which may be a large enough time gap for tumor progression or the resolution of inflammation (from steroid therapy).

II.E. Tags for validation

For certain pairs of images, homologous landmark points were chosen using the MINC tool *register* by one or multiple experts. The mean Euclidean distance between the corresponding points enables a quantitative estimation of the misalignment between the two images and can be used to validate registration techniques.

III. RESULTS

The MNI BITE database can be found in Ref. 40. The data are free and not password protected. The website also includes a few examples of how to view and manipulate the data with the MINC tools. Some of the images provided have already been used for earlier publications (see Sec. IV). For that reason, the data are divided into the following groups, each with its own characteristics and features.

III.A. Group 1: pre- and postresection ultrasound images

This group contains 2D and 3D ultrasound images acquired before and after tumor resection. Table III summarizes the ultrasound data. For each patient, more than one sweep was acquired pre- and postresection, and these sweeps are represented with lowercase letters in the second and third rows of Table III. For example, patient #7 had five preresection sweeps represented by the letters a–e and six postresection sweeps represented by the letters u–z. During the first patient's surgery, the reference was accidentally moved, and the postresection ultrasound images were not accurately tracked and thus not included here. For each patient, one of the pre- and one of the postresection sweeps are underlined, representing those for which we have ten homologous

TABLE III. Summary of ultrasound data. First row is the patient number. Second row is the preresection ultrasound sweeps (lowercase letters starting with a). Third row is the postresection ultrasound sweeps (lowercase letters starting with u). For each patient, the underlined letters form a pair for which validation points were chosen. Fourth row is the mean distance between the pair (mm). Fifth row indicates whether the surgical cavity had Surgicel and/or Tisseel when imaging.

Patient No.	1	2	3	4	5	6	7	8	9	10	11	12	13	14
Preresection sweeps	a b c d	**a** b c	a b **c**	**a** b c	**a** b c	**a** b c d	a **b** c d e	a **b** c	a **b** c	**a** b c	**a** b c d	a **b** c d	a **b**	a **b** c
Postresection sweeps	—	**u** v	u v w **x** y	**u** v w	u **v**	**u** v w x	u v w **x** y z	u **v** w	**u**	**u** v w[a]	u **v** w x	u v **w**	u v **w**	u **v** w
Pre-post initial distance	—	2.3	3.4	4.6	4.1	2.3	3.4	2.5	2.2	3.9	2.7	10.5	1.6	2.2
Surgicel and/or Tisseel		Yes	Yes	Yes	Yes	No	No	No	No	Yes	No	Yes	No	Yes

[a]Note that, for patient #10, two sweeps were done after the resection (u,v), and then the surgeon continued the resection and acquired one last sweep (w).

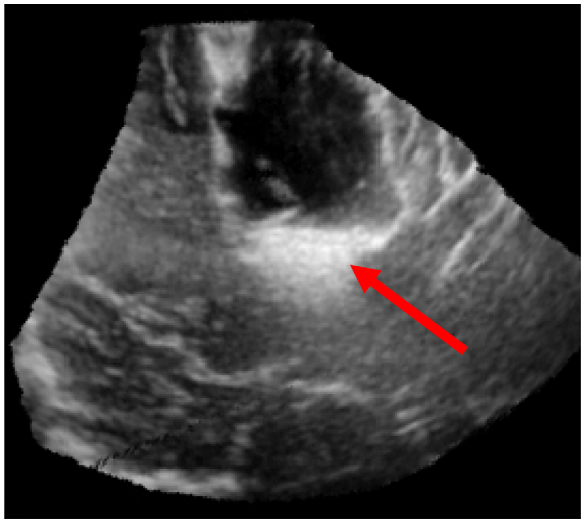

FIG. 4. Ultrasound image showing artifact caused by the presence of Surgicel in the resection cavity in patient #12. The hypoechoic region in the upper part of the image is the resection cavity and the hyperechoic artifact in the bottom of the cavity is Surgicel (red arrow).

landmarks chosen by a neuroradiologist (D.A.). The fourth row of Table III shows the mean distance between the homologous points of the underlined sweeps located in the same column.

In addition, to evaluate the reproducibility of the point picking procedure, we kept the same points on the preresection ultrasound but chose again the corresponding points on the same postresection ultrasound sweep for patients #7 and #10. Therefore, two set of tags are found in the database for these two patients. Note that, for patient #10, two sweeps were done after the resection (u,v), and then the surgeon continued the resection and acquired one last sweep (w).

The last row of Table III indicates the presence of Surgicel (Ethicon, Inc., a Johnson & Johnson company; Somerville, NJ) or Tisseel (Baxter, Deerfield, IL). Surgicel is a surgical hemostat composed of oxidized cellulose and Tisseel is a fibrin adhesive. Both can be used in the surgical cavity and often create major artifacts in the postresection ultrasound (see Fig. 4). In our study, for 7 out of 13 patients (#2, #3, #4, #5, #10, #12, and #14), the postresection ultrasounds were done with one or the other in the resection cavity, creating a hyperechoic artifact.

Figure 5 shows two sweeps acquired before the resection for patient #6, as they were initially positioned by the tracking device. As the figure illustrates, the two sweeps do not cover exactly the same anatomy and, therefore, overlap at different degrees.

Figure 6 shows pre- and postresection ultrasound images for patient #6, as they were initially positioned by the tracking device. In the combined image (right), a slight misalignment can be seen around the falx/septum/lateral ventricle area (green arrow). This misalignment is in part due to calibration errors but mostly because the brain shifts after a large tumor resection.

III.B. Group 2: preoperative MR and preresection ultrasound images

This group contains 14 pairs of preoperative MR and preresection ultrasound images (2D and 3D). For each pair, homologous landmarks were chosen by two experts (D.L.C. and L.M.). In the context of a previous paper,[21] data for patients up to #6 were tagged by a third expert (C.H.). In this group, both the MR and ultrasound images were transformed into the MNI Talairach-like brain-based coordinate space (orientation and position only, no scaling),[22] as the manual taggers found it easier to visualize the MR image in that frame of reference. The database contains the necessary transformations to map: (1) the MR images back into the native scanner space as in group 3 and (2) the ultrasound images back into native space as in group 1. Table IV shows the number of tags chosen for each case and the initial distance between the MR and ultrasound images according to these tags. The initial distance was computed by taking into account all available tags (see second column) for each case.

For each preoperative MR image in this category, a manual segmentation of the tumors is also provided in the database. We thought it would be useful to visually locate the tumor for nonexperts as well as for some registration algorithms.

Figure 7 shows two pairs of MR and ultrasound images. Note how similar the tumor features and components look in the two modalities for patient #4, but how different the tumor looks in patient #3.

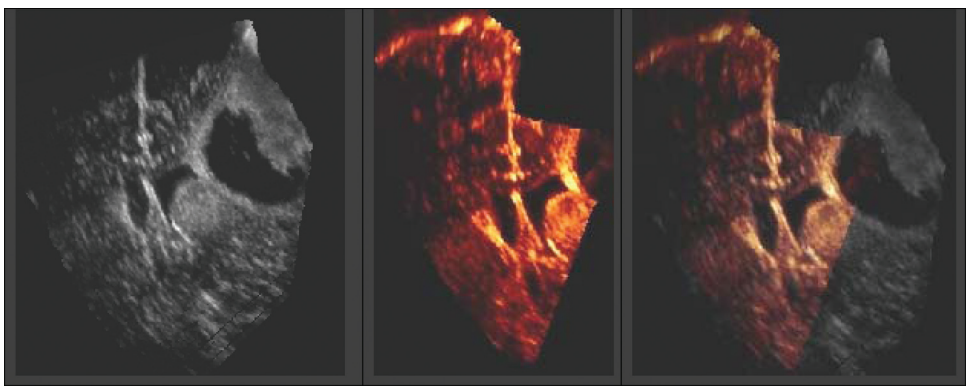

FIG. 5. Reslices of two preresection ultrasounds sweeps for patient #6. Left: sweep #6a. Center: sweep #6b. Right: sweep #6a overlaid on sweep #6b.

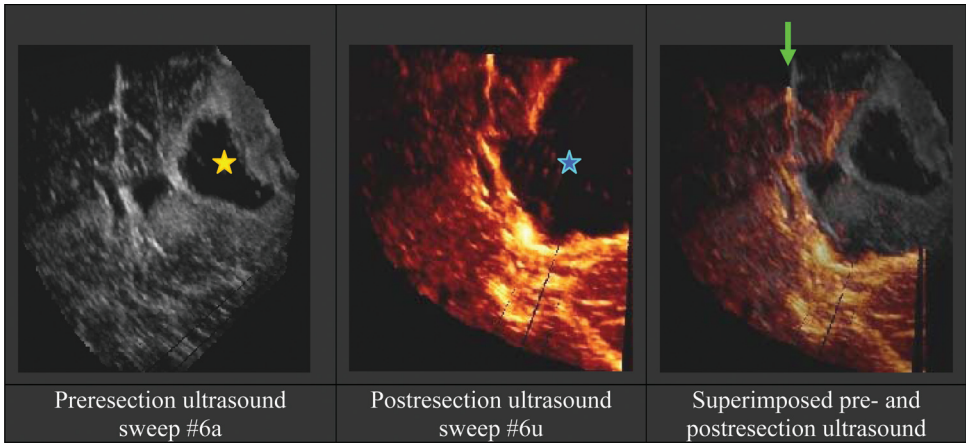

FIG. 6. Reslices of two ultrasound volumes acquired for patient #6. Left: preresection ultrasound of a tumor with a large cyst (yellow star). Center: postresection ultrasound. The resection cavity (blue star) is very large and includes the lateral ventricle. Right: superimposed pre- and postresection ultrasound. A small visible shift can be seen between the two (green arrow).

III.C. Group 3: pre- and postresection MR images

This group includes MR images taken at two different time points: before and after surgery. The MR images are provided in their original scanner frame of reference. Except for anonymization, these images were not subject to any other preprocessing. The database provides patient–MR image registration for each preoperative MR image to allow the reader to transform the preoperative MR image into the same frame of reference as the ultrasound data used in group 1. The data for this group were described in Table II. Figure 8 shows example images for patient #11. In the figure, both MR images are T1w gadolinium-enhanced images. However, as shown in Table II, the preoperative and postoperative data often have different resolutions. The images in this group have not been previously used in a publication and, therefore, do not have any tags available for registration validation. Selecting homologous landmarks on MR images with different slice thicknesses can be difficult. We suggest using visual ratings for the validation of registration methods using the images in this group.

TABLE IV. Summary of validation tags for the data in group 2. First column is the patient number. Second column is the number of tags available for each case. Third column is the mean distance (mm) between the MR and ultrasound images and range computed from these tags.

Patient No.	No. of tags	Mean initial distance (range)
1	37	4.9 (1.0–9.1)
2	35	6.5 (1.9–9.0)
3	40	9.4 (6.3–12.8)
4	32	3.9 (1.0–6.1)
5	31	2.6 (0.5–6.9)
6	37	2.3 (0.2–4.4)
7	19	3.0 (0.3–6.3)
8	23	3.6 (0.03–8.4)
9	21	5.1 (2.5–7.6)
10	25	3.0 (5.3–0.8)
11	25	1.5 (0.6–3.5)
12	21	3.7 (0.9–7.0)
13	23	5.1 (1.5–10.4)
14	23	3.8 (1.2–5.7)

IV. DISCUSSION

This database, containing both MR and ultrasound images of patients with brain tumors, is unique, and we believe it can become the basis of a large quantity of research. Here are a few ideas of potential research uses for the data.

IV.A. Group 1: pre- and postresection ultrasound images

The 3D ultrasound images in this group have previously been used for nonlinear registration of pre- and postresection ultrasound images in Mercier *et al.*[23] The images and tags can be reused for other registration approaches. For example, our previous procedure[19] could be extended further by first combining all sweeps at each time point before registration. Another possibility would be to combine all sweeps acquired at the same time point by spatial compounding to provide ultrasound images with a larger field of view.[24–26] These larger-field-of-view ultrasounds could also be used for registration, although the tags might not be valid in this case and might need to be redone.

IV.B. Group 2: preoperative MR and preresection ultrasound images

We have already published a paper on linear registration of MR and 3D ultrasound images using the data in this group and earlier cases for which we do not have patient consent for online distribution.[27–29] With the validation points provided, the images in this group can be reused in other papers on MR–ultrasound image registration,[30,31] such as nonlinear approaches. Another possibility would be to register MR images with the 2D ultrasound slices instead of the 3D reconstructed ultrasound volumes. However, the tags provided (in 3D) could not be used to validate such an approach.

IV.C. Group 3: pre- and postresection MR images

The images in this group have never been used for publication but would be suitable for papers focusing on MR–MR

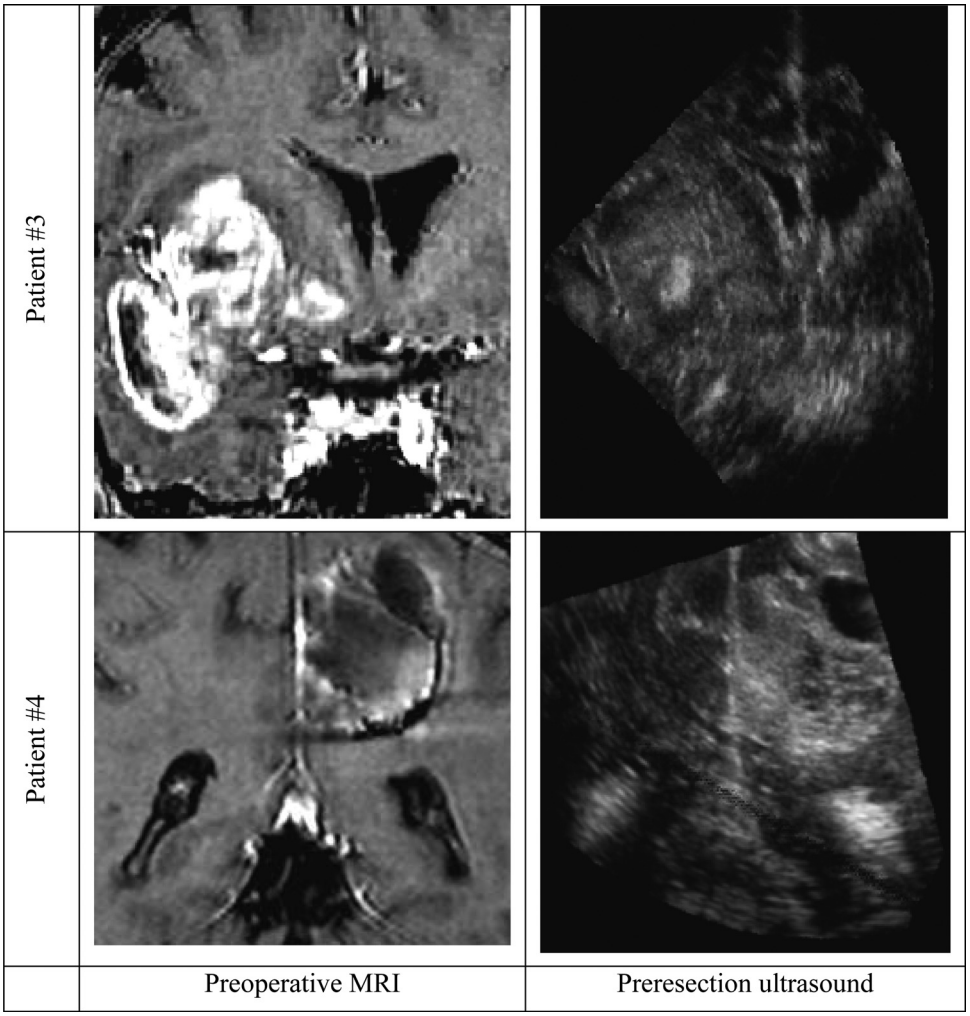

FIG. 7. Left: reslice of preoperative MR images. Right: corresponding reslice of the preresection ultrasounds for patient #3 (upper row) and patient #4 (lower row).

registration of images taken at different time points, similar to work previously published.[32–37] This topic has gained popularity since the advent of commercial intraoperative MR imaging systems, and brain tumor resection is a particularly challenging problem, as it involves tissue resection and nonlinear brain shift.

IV.D. Other possibilities

Other possible studies include 3D ultrasound reconstruction from 2D images[16,38,39] or registration of postresection ultrasound images with postoperative MR images, which, to our knowledge, has never been done.

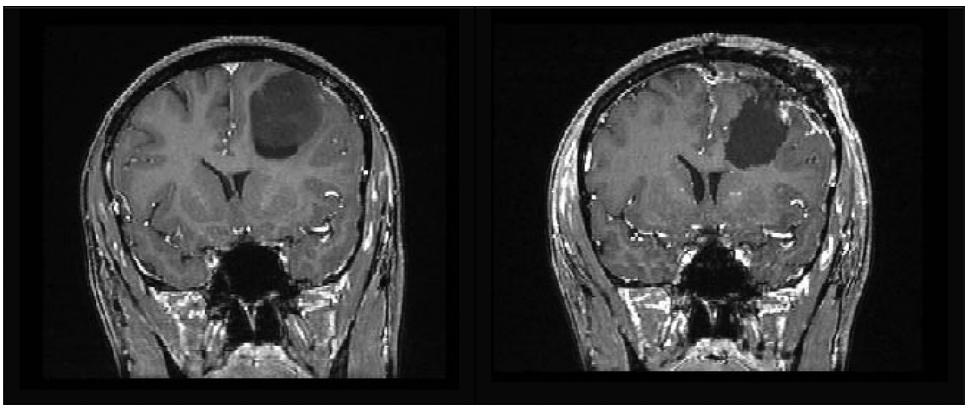

FIG. 8. MR images for patient #11. Left: preoperative MRI. Right: postoperative MRI.

V. CONCLUSIONS

We present a unique database containing pre- and postoperative MR images as well as intraoperative ultrasound images of 14 brain tumor patients. This free database will provide technical scientists with easily accessible clinical images and validation points. Such a common set of data can be used to evaluate different methods and, as such, enables direct comparison of different image processing algorithms. This database will, we hope, trigger multiple studies that will eventually benefit brain tumor patients by allowing their surgeons to better visualize the brain before, during, and after surgery.

ACKNOWLEDGMENTS

The authors would like to thank the patients who allowed distribution of their images, Dr. Hassan Rivaz for his comments on the manuscript, and Sean Chen for the right picture in Fig. 1. This work was financed by the *Fonds québécois de la recherche sur la nature et les technologies*, the Canadian Institutes of Health Research (MOP-97820), and the Natural Science and Engineering Research Council of Canada, the Franco Di Giovanni Foundation, B-Strong, the Alex Pavanel family, the Raymonde and Tony Boeckh Funds for brain tumour research, the Montreal English School Board, the Brainstorm Foundation, the Colannini Foundation, and the Brain Tumor Foundation of Canada. Dr. R. F. Del Maestro holds the William Feindel Chair in Neuro-Oncology at McGill University.

[a]Author to whom correspondence should be addressed. Electronic mail: louis.collins@mcgill.ca; Telephone: +1 514.398.4227; Fax: +1 514.398.2975.

[1]M. Prastawa, E. Bullitt, and G. Gerig, "Simulation of brain tumors in MR images for evaluation of segmentation efficacy," Med. Image Anal. **13**(2), 297–311 (2009).
[2]C. Cocosco, V. Kollokian, R.-S. Kwan, and A. Evans, "Brainweb: online interface to a 3D MRI simulated brain database," NeuroImage **5**(4) S425 (1997).
[3]D. L. Collins *et al.*, "Design and construction of a realistic digital brain phantom," IEEE Trans. Med. Imaging **17**(3), 463–468 (1998).
[4]S. Chen *et al.*, "An anthropomorphic polyvinyl alcohol triple-modality brain phantom based on Colin27," in *Medical Image Computing and Computer-Assisted Intervention—MICCAI 2010*, edited by T. Jiang *et al.* (Springer, Berlin/Heidelberg, 2010), pp. 92–100.
[5]The Internet Brain Segmentation Repository (IBSR), Available from: http://www.cma.mgh.harvard.edu/ibsr/.
[6]D. W. Shattuck *et al.*, "Construction of a 3D probabilistic atlas of human cortical structures," Neuroimage **39**(3), 1064–1080 (2008).
[7]BrainMap, Available from: http://brainmap.org/.
[8]A. C. Evans, "The NIH MRI study of normal brain development," Neuroimage **30**(1), 184–202 (2006).
[9]K. A. Johnson and J. A. Becker, The Whole Brain Atlas. Available from: www.med.harvard.edu//AANLIB/home.html.
[10]S. G. Mueller *et al.*, "The Alzheimer's disease neuroimaging initiative," Neuroimaging Clin N. Am. **15**(4), 869–877 (2005).
[11]D. S. Marcus *et al.*, "Open Access Series of Imaging Studies (OASIS): Cross-sectional MRI data in young, middle aged, nondemented, and demented older adults," J. Cognit. Neurosci. **19**(9), 1498–1507 (2007).
[12]D. Marcus *et al.*, "Open Access Series of Imaging Studies (OASIS): Cross-Sectional MRI data in young, middle aged, nondemented, and demented older adults," J. Cognit. Neurosci. **19**, 1498–1507 (2010).
[13]P. Neelin, "The MINC file format:from bytes to brains," Neuroimage **7**(4), S786 (1998).
[14]L. Mercier *et al.*, "New prototype neuronavigation system based on preoperative imaging and intraoperative freehand ultrasound: System description and validation," Int. J. Comput. Assist. Radiol. Surg. **6**(4), 507–522 (2011).
[15]D. G. Gobbi, R. M. Comeau, and T. M. Peters, "Ultrasound probe tracking for real-time ultrasound/MRI overlay and visualization of brain shift," in *MICCAI 1999*. (Springer, Cambridge, UK, 1999), Lecture Notes in Computer Science.
[16]O. V. Solberg *et al.*, "Freehand 3D ultrasound reconstruction algorithms—A review," Ultrasound Med. Biol. **33**, 991–1009 (2007).
[17]D. R. Enzmann *et al.*, "Tumors of the central nervous system studied by computed tomography and ultrasound," Radiology **154**(2), 393–399 (1985).
[18]P. D. Le Roux *et al.*, "A comparison between preoperative magnetic resonance and intraoperative ultrasound tumor volumes and margins," J. Clin. Ultrasound **22**(1), 29–36 (1994).
[19]L. Mercier *et al.*, "Experience using intraoperative 3D ultrasound in conjunction with preoperative MRI in brain tumor surgery." in *5th Annual Scientific Meeting of the Society for Neuro-Oncology*, 2010, Montreal, Canada.
[20]J. P. McGahan *et al.*, "Brain gliomas: Sonographic characterization," Radiology **159**(2), 485–492 (1986).
[21]L. Mercier *et al.*, "Comparing two approaches to rigid registration of three-dimensional ultrasound and magnetic resonance images for neurosurgery," Int. J. Comput. Assist. Radiol. Surg. **7**(1), 125–136 (2012).
[22]D. L. Collins *et al.*, "Automatic 3D intersubject registration of MR volumetric data in standardized Talairach space," J. Comput. Assist. Tomogr. **18**(2), 192–205 (1994).
[23]L. Mercier *et al.*, "Registering pre- and post-resection 3D ultrasound for improved residual brain tumor localization," Ultrasound Med. Biol. (submitted).
[24]J. F. Krucker *et al.*, "3D spatial compounding of ultrasound images using image-based nonrigid registration," Ultrasound Med. Biol. **26**(9), 1475–1488 (2000).
[25]T. C. Poon and R. N. Rohling, "Three-dimensional extended field-of-view ultrasound," Ultrasound Med. Biol. **32**(3), 357–369 (2006).
[26]R. N. Rohling, A. H. Gee, and L. Berman, "Three-dimensional spatial compounding of ultrasound images," Med. Image Anal. **1**(3), 177–193 (1997).
[27]L. Mercier *et al.*, "Rigid registration of 3D ultrasound and MRI: Comparing two approaches on nine tumor cas," in *CIM Symposium on Brain, Body and Machine*, 2010 (Springer, Montreal, Canada, 2010).
[28]L. Mercier *et al.*, "Comparing two approaches to rigid registration of three-dimensional ultrasound and magnetic resonance images for neurosurgery," Int. J. Comput. Assist. Radiol. Surg. **7**, 125–136 (2012).
[29]D. De Nigris *et al.*, "Hierarchical multimodal image registration based on adaptive local mutual information," in *Medical Image Computing and Computer-Assisted Intervention—MICCAI 2010*, edited by T. Jiang *et al.* (Springer, Berlin/Heidelberg, 2010), pp. 643–651.
[30]S. Ji *et al.*, "Mutual-information-based image to patient re-registration using intraoperative ultrasound in image-guided neurosurgery," Med. Phys. **35**(10), 4612–4624 (2008).
[31]A. Roche *et al.*, "Rigid registration of 3-D ultrasound with MR images: A new approach combining intensity and gradient information," IEEE Trans. Med. Imaging **20**(10), 1038–1049 (2001).
[32]L. Yixun *et al.*, "A point based non-rigid registration for tumor resection using iMRI," in *IEEE International Symposium on Biomedical Imaging: From Nano to Macro* (2010).
[33]N. Archip *et al.*, "Non-rigid alignment of pre-operative MRI, fMRI, and DT-MRI with intra-operative MRI for enhanced visualization and navigation in image-guided neurosurgery," Neuroimage **35**(2), 609–624 (2007).
[34]S. Ding *et al.*, "Semiautomatic registration of pre- and post brain tumor resection laser range data: Method and validation," IEEE Trans. Biomed. Eng. **56**(3), 770–780 (2009).
[35]P. Risholm *et al.*, "A non-rigid registration framework that accommodates resection and retraction," in *Inf Process Med Imaging IPMI*, **21**, 447–458 (2009).
[36]O. Clatz *et al.*, "Robust nonrigid registration to capture brain shift from intraoperative MRI," IEEE Trans. Med. Imaging **24**(11), 1417–1427 (2005).
[37]N. Chitphakdithai and J. Duncan, "Non-rigid registration with missing correspondences in preoperative and postresection brain images," in *Medical Image Computing and Computer-Assisted Intervention—MICCAI 2010*, edited by T. Jiang *et al.* (Springer, Berlin/Heidelberg, 2010), pp. 367–374.
[38]Q. H. Huang and Y. P. Zheng, :Volume reconstruction of freehand three-dimensional ultrasound using median filters," Ultrasonics **48**(3), 182–192 (2008).
[39]P. Coupe *et al.*, "Probe trajectory interpolation for 3D reconstruction of freehand ultrasound," Med. Image Anal. **11**, 604–615 (2007).
[40]http://www.bic.mni.mcgill.ca/BITE.